G. Vogel

A. B. A. Graf

Laboratoire de Thermique Appliquée et de Turbomachines (LTT),
EPFL,
1015 Lausanne, Switzerland

J. von Wolfersdorf

B. Weigand

Institut für Thermodynamik der Luft- und Raumfahrt,
Universität Stuttgart,
70569 Stuttgart, Germany

A Novel Transient Heater-Foil Technique for Liquid Crystal Experiments on Film-Cooled Surfaces

A novel transient measurement technique has been developed for determining the heat transfer characteristics in the presence of film cooling (heat transfer coefficient and adiabatic film-cooling effectiveness). The method is based on a transient heater foil technique, where a non-homogeneous surface heat flux is applied to the test surface. A regression analysis of multiple transient liquid crystal experiments is used to obtain the heat transfer characteristics. The method introduced here has the advantage that the (often not known) heat flux distribution at the surface is not needed for the analysis of the measured data. The method is used to study the influence of several heater foil configurations on a flat plate with film cooling, elucidating the effect of different thermal boundary conditions on film-cooling performance. The obtained data is also compared to results presented in literature and good agreement is found. [DOI: 10.1115/1.1578501]

1 Introduction

Efficient cooling methods are required in modern gas turbine designs due to excessive high turbine inlet temperatures introduced by the demand of high specific power and high cycle efficiency. Although the high temperature capabilities of the applied materials were improved over the last years, the thermal and stress environment are beyond the limit alloys can presently achieve. In order to protect the turbine blades from melting, the blades need extensive cooling. Usually a combination of internal convective cooling and external film cooling is employed. The cooling designs of these parts have to be highly efficient because a larger cooling mass flow rate degrades the thermal efficiency of the thermodynamic cycle of the gas turbine. This is especially true for the application of film cooling where a protective film of cold air is spread around the blade and large cooling mass flows are required. Because of the importance of film cooling for turbine blade design, this subject has been studied extensively over the past 35 yr (Goldstein [1,2], Leontiev [3]). Most of the studies concentrate on flat plate configurations with film injection through slots, cylindrical or shaped holes (Sinha et al. [4], Forth et al. [5]). When film cooling is considered on airfoil type flows (Ito et al. [6], Takeishi et al. [7], Drost [8]), numerical methods and correlations have been developed to predict the adiabatic film-cooling effectiveness and the increase in heat transfer coefficients. A large number of parameters influence the film cooling process such as cooling hole geometry, blowing and momentum flux ratio of the coolant and main stream turbulence effects. Several models can be found in literature (Crawford et al. [9], Weigand et al. [10], Garg [11]), albeit only for specific applications. In order to further develop the cooling schemes for gas turbine blades, high quality experimental data and the corresponding analytical and numerical methods are required.

Transient and steady-state heat transfer and film cooling effectiveness measurements using thermochromic liquid crystals (TLC) are very popular to obtain detailed full field surface information (Ireland et al. [12]). For film cooling measurements several techniques have been applied to determine the film cooling performance (adiabatic film-cooling effectiveness and increase in film cooling heat transfer coefficients) either by two separate experiments, or by a number of transient experiments. Two separate steady-state experiments were performed by Lutum et al. [13]. The increase in heat transfer coefficient due to film cooling was measured using a heater foil, the coolant temperature and the free stream temperature being equal. The adiabatic film-cooling effectiveness was additionally measured by using an adiabatic wall and by blowing with a different coolant temperature than the free stream temperature. The heater foil covered the region before and after the injection holes with some unheated region around the holes. Regression analysis on multiple transient liquid crystal measurements using rapidly changing free stream temperature, generally performed by the rapid insertion of a preconditioned model or by using heater grids in the main flow, or various coolant temperatures were reported by Reiss [14] and Dui et al. [15]. Transient heater-foil techniques with liquid crystal thermography were applied for heat transfer investigations by von Wolfersdorf et al. [16] and Turnbull et al. [17]. Since no film-cooling holes were considered, the full surface under investigation was covered with the heated layer. In case of film cooling, transient measurements using heater foils were applied for slots by Farmer et al. [18] and for a row of holes by Seager et al. [19], the heater-foil being then applied in the area behind the holes.

The aforementioned different heater-foil arrangements cause different thermal boundary conditions for the film cooling situation. Therefore, a new transient heater foil method was introduced by Vogel et al. [20], which is able to determine the film-cooling effectiveness and the heat transfer augmentation simultaneously even for nonuniform heat flux situations (e.g., film-cooling holes in the heater foil) using multiple transient experiments and regression analysis. The applicability of this method was shown for one film cooling experiments on a flat plate with cylindrical holes and two heater-configurations with longitudinal and transverse electrical current supply.

The objective of the present paper is to introduce a new transient heater foil method for liquid crystal experiments on film cooled surfaces. An analytical model and its numerical resolution are first derived. The experimental setup is then described as much as a measurement errors analysis. Furthermore, the present paper studies the influence of four different heater-foil configurations and therefore different thermal boundary conditions on the film

Contributed by the International Gas Turbine Institute and presented at the International Gas Turbine and Aeroengine Congress and Exhibition, Amsterdam, The Netherlands, June 3–6, 2002. Manuscript received by the IGTI October 10, 2001; revised manuscript received October 29, 2002. Paper No. 2002-GT-30552. Review Chair: E. Benvenuti.

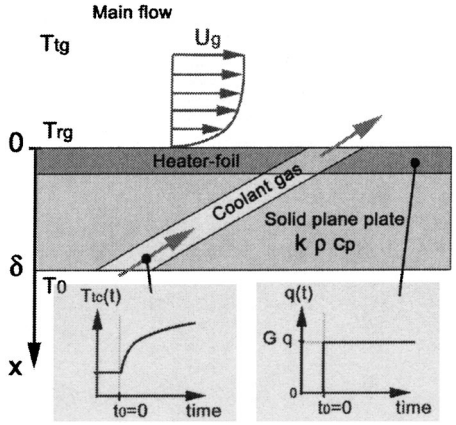

Fig. 1 Schema of the solid plane plate with the heater-foil, the coolant injection, cooling holes, the main gas flow, and some relevant physical quantities

cooling performance. This point is of major importance for the transfer of experimental data in literature to actual film cooling configurations in gas turbines.

2 Theoretical Investigation of the Measurement Technique

2.1 Model. Figure 1 gives an overview of the considered model. A coolant fluid is injected into the main flow of gas over a flat plate. The latter is covered by a thin heater foil. At $t=0$, the plate is suddenly exposed to a heat flux through the foil, causing a temperature change in the wall of the plate. The evolution of the temperature field in the plate is assumed to be one-dimensional and the heat diffusion conduction equation in the plate in the absence of heat sources can be written as

$$\frac{\partial T(x,t)}{\partial t}=\alpha\frac{\partial^2 T(x,t)}{\partial x^2},\quad \alpha=\frac{k}{\rho c_p} \tag{1}$$

The heater-foil is supposed to be infinitely thin compared to δ. Its effect is thus taken into account in the boundary conditions and not in the heat conduction equation itself. This same assumption allows the plate to be considered as homogenous.

The initial condition ($t=0$) is given by

$$T(x,0)=T_0 \tag{2}$$

whereas the boundary condition at the plate surface ($x=0$) is obtained using an energy balance

$$\dot{q}_W(t)=-k\frac{\partial T(0,t)}{\partial x}-h(T_{aw}(t)-T(0,t)) \tag{3}$$

where $T_{aw}(t)$ stands for the adiabatic wall temperature. This value can be replaced by the adiabatic film-cooling effectiveness, which is defined by

$$\eta=\frac{T_{aw}(t)-T_{rg}}{T_{tc}(t)-T_{tg}} \tag{4}$$

where T_{tg} and T_{rg} are determined using the flow conditions of the main stream of gas. Furthermore, it is assumed that the plate can be treated as half-infinite (Vogel et al. [21]), i.e., the measurement time is so short that a heat pulse generated at the upper surface ($x=0$) will not reach the lower one ($x=\delta$). This can be expressed by the condition

$$T(x\to\infty,t)=T_0 \tag{5}$$

Solving Eq. (4) for $T_{aw}(t)$ and substituting it into Eq. (3) yields

$$\dot{q}_W(t)=-k\frac{\partial T(0,t)}{\partial x}+h(T(0,t)-T_{rg})+h\,\eta(T_{tg}-T_{tc}(t)) \tag{6}$$

Equation (1) can be solved analytically under the conditions given by Eqs. (2), (5), and (6) using the Laplace transform technique as described by Carslaw et al. [22]. With $T^*(x,t)=T(x,t)-T_0$, the following transformed quantities are obtained:

$$\begin{cases}\hat{T}^*(x,s)=\sigma\exp\left(-\sqrt{\dfrac{s}{\alpha}}x\right)\\ \hat{q}_W(s)=-k\dfrac{\partial\hat{T}^*(0,s)}{\partial x}+h\hat{T}^*(0,s)+\dfrac{h(\eta T_{tg}+T_0-T_{rg})}{s}-h\,\eta\hat{T}_{tc}(s)\end{cases} \tag{7}$$

where σ is an integration constant. In order to determine the latter, the following assumptions are made: at $t=0$ a step in the surface heat flux is generated by the heater-foil and at the same time, a coolant gas is injected at a constant blowing ratio and with a given temperature evolution in time as defined in the following:

The coolant temperature is a function of time since the cooling fluid is transferred from the plenum chamber to the test section, this transfer being accompanied by a heat loss. The temperature rise of the coolant is assumed to follow an expression as:

$$T_{tc}(t)=a\exp(bt)+ct+d\sqrt{t} \tag{8}$$

where a, b, c, and d are constants fitted to the experimental profile of $T_{tc}(t)$. The surface heat flux follows a step function:

$$\begin{cases}\dot{q}_W(t\leqslant 0)=0\\ \dot{q}_W(t>0)=Gq\end{cases} \tag{9}$$

where G stands for the known gain with respect to an unknown reference heat flux q. Under the assumptions of Eqs. (8) and (9), the system of Eq. (7) has the following solution:

$$\hat{T}^*(x,s)=\left[\frac{Gq}{s}-\frac{h(\eta T_{tg}+T_0-T_{rg})}{s}+h\,\eta\left(\frac{a}{s-b}+\frac{c}{s^2}+\frac{\sqrt{\pi}d}{2\sqrt{s^3}}\right)\right]\frac{\exp\left(-\sqrt{\dfrac{s}{\alpha}}x\right)}{h+k\sqrt{\dfrac{s}{\alpha}}} \tag{10}$$

The inverse Laplace transform of the foregoing expression evaluated at $x=0$ yields for the wall temperature distribution

$$T_w(t)=A+\eta B+qC \tag{11}$$

where

$$A = T_0 + (T_{rg} - T_0)(1 - \exp(\beta^2)\operatorname{erfc}(\beta))$$

$$B = -T_{tg}(1 - \exp(\beta^2)\operatorname{erfc}(\beta)) + \frac{h}{k}\left[\frac{a\exp(bt)}{2}\mu - \frac{a\alpha}{\frac{h}{k}\alpha - \frac{kb}{h}}\exp(\beta^2)\operatorname{erfc}(\beta)\right]$$

$$-\frac{h}{k}\left[\frac{c}{\alpha\left(\frac{h}{k}\right)^3}\left(\exp(\beta^2)\operatorname{erfc}(\beta) - \sum_{r=0}^{2}\frac{(-\beta)^r}{\Gamma\left(\frac{r}{2}+1\right)}\right) - \frac{d\sqrt{\pi}}{2\sqrt{\alpha}\left(\frac{h}{k}\right)^2}\left(\exp(\beta^2)\operatorname{erfc}(\beta) - \sum_{r=0}^{1}\frac{(-\beta)^r}{\Gamma\left(\frac{r}{2}+1\right)}\right)\right]$$

$$C = \frac{G}{h}(1 - \exp(\beta^2)\operatorname{erfc}(\beta)) \tag{12}$$

with $\beta^2 = \alpha(h/k)^2$ $t \neq bt$ and:

$$\mu = \begin{cases} \dfrac{\sqrt{\alpha}}{\frac{h}{k}\sqrt{\alpha} + \sqrt{b}}\operatorname{erfc}(-\sqrt{bt}) + \dfrac{\sqrt{\alpha}}{\frac{h}{k}\sqrt{\alpha} - \sqrt{b}}\operatorname{erfc}(\sqrt{bt}) & \text{when } b \geqslant 0 \\ \dfrac{2\sqrt{\alpha}}{\left(\frac{h}{k}\right)^2\alpha + b}\left(\dfrac{h}{k}\sqrt{\alpha} + 2\sqrt{\dfrac{-b}{\pi}}\left(\displaystyle\int_0^{\sqrt{-bt}}\exp(t^2)dt\right)\right) & \text{when } b < 0 \end{cases} \tag{13}$$

When considering the case of no film cooling (i.e., $\eta = 0$) and a constant heat flux, the foregoing equations reduce to the expression given by von Wolfersdorf et al. [16].

2.2 Regression. All parameters in Eq. (11) are assumed to be known *a priori* or measured except for h, η, and q. These unknown quantities are determined below by a nonlinear least-square regression using the transient experimental data. The latter includes temperature-time data pairs which are given by the coating of narrow-band liquid crystals applied on the plate and can be written as $(T^i_{LC}, t^i_{LC})|^N_{i=1}$ where i indexes the $N \geqslant 3$ independent experiments such that

$$T_w(t^i_{LC}) = T^i_{LC}, \quad \forall i = 1,..,N \tag{14}$$

The foregoing holds locally since the value of q is inhomogeneous across the surface of the plate as it depends upon the influence of the cooling holes and upon the possible variation in thickness of the heater-foil. For $N = 3$, Eq. (14) yields exactly a solution triplet, if the latter exists. However, for $N > 3$, the problem is overdefined and an optimal solution, if it exists, has to be sought. This solution should fit best all the N equations together, without necessarily satisfying each of them exactly. The foregoing problem thus reduces to minimizing the following error function:

$$\varepsilon = \frac{1}{2}\|\vec{T}_w(t_{LC}) - \vec{T}_{LC}\|^2 = \frac{1}{2}\|\vec{A} + \eta\vec{B} + q\vec{C} - \vec{T}_{LC}\|^2 \tag{15}$$

where each component of a vector corresponds to a distinct experiment and where $\|\vec{x}\|^2 = \langle\vec{x}|\vec{x}\rangle$, $\langle .|. \rangle$ being the Euclidean scalar product for $\vec{x} \in \mathbb{R}^N$. The foregoing expression is minimal when:

$$\vec{\nabla}\varepsilon = 0 \Rightarrow \frac{\partial\varepsilon}{\partial\eta} = 0, \quad \frac{\partial\varepsilon}{\partial q} = 0, \quad \frac{\partial\varepsilon}{\partial h} = 0 \tag{16}$$

which is a necessary but nonsufficient condition.

In the context of Eq. (11), the above three-parameter optimization process may be reduced to a one-parameter one. For this, η is expressed as a function of the two remaining unknowns as

$$\frac{\partial\varepsilon}{\partial\eta} = 0 \Rightarrow \eta(h,q) = \frac{\langle\vec{T}_{LC} - q\vec{C} - \vec{A}|\vec{B}\rangle}{\|\vec{B}\|^2} \tag{17}$$

Subsequently q is determined with respect to h as follows:

$$\frac{\partial\varepsilon}{\partial q} = 0 \Rightarrow q(h) = \frac{\left\langle \vec{T}_{LC} - \vec{A} - \dfrac{\langle\vec{T}_{LC} - \vec{A}|\vec{B}\rangle}{\|\vec{B}\|^2}\vec{B} \,\middle|\, \vec{\omega}\right\rangle}{\|\vec{\omega}\|^2} \quad \text{where}$$

$$\vec{\omega} = \vec{C} - \frac{\langle\vec{C}|\vec{B}\rangle}{\|\vec{B}\|^2}\vec{B} \tag{18}$$

Equations (17) and (18) are inserted into Eq. (15), yielding an error function dependent solely upon h. This one-dimensional minimization may be done by classical methods of numerical analysis (Isaacson et al. [23]) such as the bisection rule. Once the optimal value of h is determined, the remaining unknowns are computed using Eqs. (18) and (17), respectively.

3 Validation Experiments

3.1 Test Facility. Experiments are carried out in an open low speed wind tunnel with a square cross section of 100 mm $\times$100 mm and a total length of 1500 mm. In order to have good optical access and low thermal conductivity, the walls of the channel are made out of 15-mm-thick Perspex. The air flow is generated by two electrical fans mounted in serie followed by a settling chamber and a convergent nozzle as represented in Fig. 2.

The flat plate test section is mounted into the bottom wall of the channel at 10 hydraulic diameters from the square channel inlet. The test section, 250 mm in length and a wall thickness of $\delta = 25$ mm, covers the complete width of the channel (100 mm). At the start of the test plate a small step is installed in order to guarantee a turbulent boundary layer of the main gas flow on the test section. The latter consists of a flat plate film-cooled by a row of five cylindrical holes of $D = 5\text{e}{-3}$ m diameter. This row of holes is located at 20 hole diameters from the end of the plate. The five holes are centered in the transversal (span-wise) direction of the squared channel with a pitch of $P/D = 3.5$. The axis of the holes is aligned to the channel flow direction with an exit angle of 30° to the surface of the flat plate. The ratio between the length of the hole L_d and its diameter D is $L_d/D > 3$.

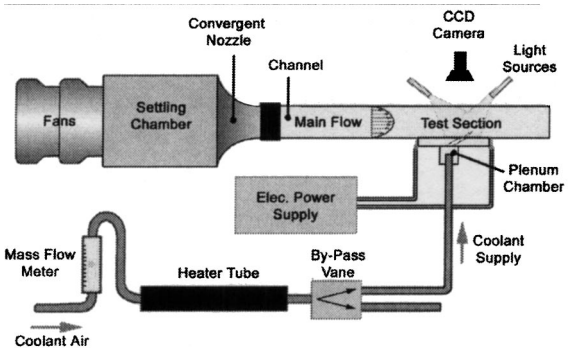

Fig. 2 Schematic drawing of the test facility and the devices present around the test section

The plenum chamber, containing the coolant and allowing its injection into the test section, is fixed to the bottom part of the test section. Coolant is supplied to the plenum chamber by an orifice located on the lateral right-hand side relative to the main flow direction in the channel. The coolant blowing ratio is adjusted and measured by a graduated glass flow meter. The temperature of the coolant is adjusted by an electrical heater tube mounted downstream of the glass flow meter. A by-pass vane mounted at the exit of the heater tube allows the preconditioning of the coolant flow before its injection into the plenum chamber where a thermocouple measures the coolant temperature during the experiments.

A nickel-chrome heater-foil of 20 μm thickness is glued onto the upper surface of the test section. The foil is connected to an electrical power supply through copper cables and bus bars. Thermocouples mounted slightly under the upper surface of the plate (for the sake of electrical insulation with the heater foil) and on its lower surface are used to monitor the homogeneity of the initial surface temperature and to verify the half infinite model assumption.

A black coating layer (Hallcrest BB-G1) followed by a thermochromic narrow band liquid crystals layer (Hallcrest BM/R36C1W) and a varnish protection layer (Hallcrest AQB-2) are applied on the heater foil. A thermocouple mounted (with a 3M Kapton tape) on top of these layers is used for the hue-temperature calibration of the liquid crystals. Cold light sources directed by optical fibers are used for the illumination of the test section. Hue value variations on the surface are recorded during the transient experiment by a 25 Hz color CCD camera mounted perpendicular to the test section and viewing through the upper channel wall. At any position on the plate, the time t_{LC} needed from the beginning of the transient experiment to reach a specific surface temperature T_{LC} is obtained by performing a data reduction of the hue video sequence (Vogel et al. [24]). An LED, mounted close to the test section and used to determine the beginning of the transient experiment on the video sequences, is triggered by the activation of the power supply connected to the heater-foil. The same trigger signal is also used to activate the bypass vane, hence synchronizing the coolant flow injection with the surface heat flux generation.

3.2 Test Cases for Validation. Experiments are performed in the above wind tunnel with an exit flow velocity of about $U_g = 22$ m/s and a total gas temperature of about $T_{tg} = 296$ K. Air is used as coolant and the film-cooling blowing ratio is set to BR $= 0.3$. The initial temperature of the test section is in the same range as the total gas temperature and a specific hue value of the narrow-band liquid crystals is calibrated for $T_{LC} = 309.2$ K. The coolant is preconditioned with temperatures varying from 298 to 323 K. The variable amount of heat flux applied during the N transient experiments is chosen in order to have a time event detection neither too short ($t_{LC} > 2$ s) because of the rapid evolution of T_w at the beginning of the transient test, nor too long ($t_{LC} < 1200$ s) in order to respect the half-infinite assumption. Numerical simulations of the temporal evolution of T_w were performed in order to assess the range of t_{LC} for the experiments. For every flat plate configuration, a total of nine experiments ($N = 9$) are performed, consisting of three different heat flux ratios combined with three different coolant temperature preconditioning. Four different heater-foil configurations as shown in Fig. 3 are investigated.

Case 1: Longitudinal Electrical Current. One pair of bus bars is connected perpendicular to the flow direction forcing a global

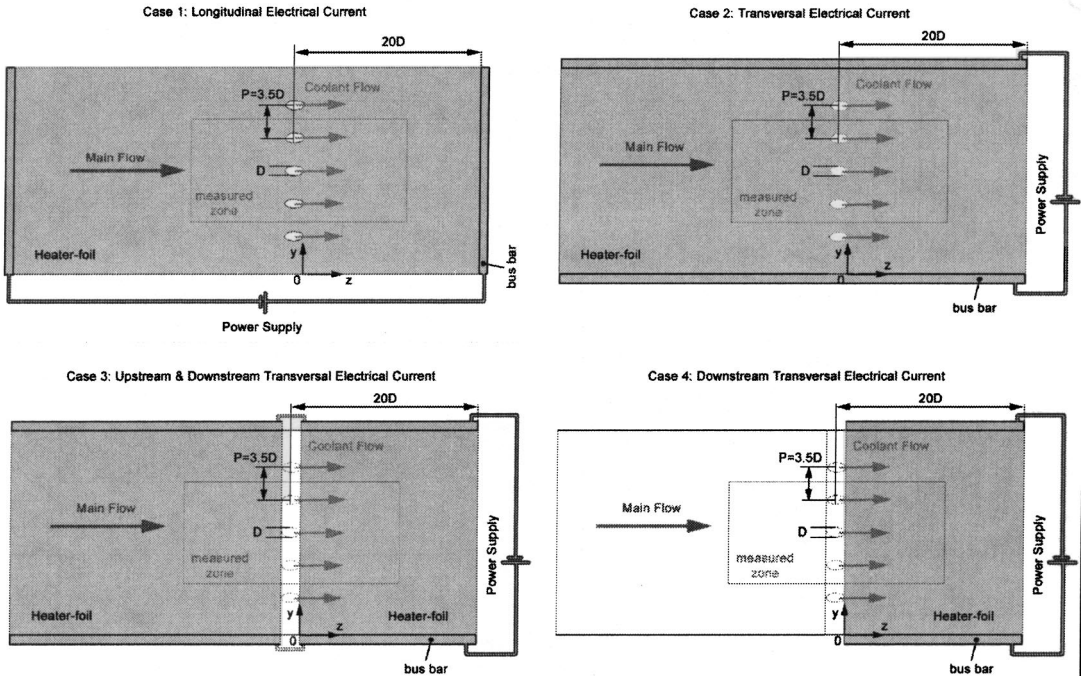

Fig. 3 Film-cooled flat plate heater-foils and bus bars configurations

longitudinal electrical current in the foil. This configuration generates a nonhomogeneous heat flux distribution with higher values in between the holes as a consequence of the reduced conductible surface (conservation of electric charge).

Case 2: Transversal Electrical Current. One pair of bus bars is connected parallel to the flow direction forcing a global transversal electrical current in the foil. This configuration also generates a nonhomogeneous heat flux distribution with lower values in between the holes.

Case 3: Upstream and Downstream Transversal Electrical Current. Two pairs of bus bars are connected parallel to the flow direction forcing a global transversal electrical current in two foils, one upstream and the other downstream of the row of cooling holes. This configuration generates two homogeneous heat fluxes, the latter being however different.

Case 4: Downstream Transversal Electrical Current. One pair of bus bars is connected parallel to the flow direction forcing a global transversal electrical current in the foil downstream of the row of cooling holes, generating thus a homogeneous heat flux.

Since the measurement technique proposed in this paper is developed for heater-foil experiments with an unknown surface heat flux distribution q, the first two cases provide a good illustration of its usefulness and general applicability, while the last two cases allow to determine the influence of the heater foil on the film-cooling measurements.

4 Measurement Errors

The approach used here for the measurement error analysis is similar to the one described by Kline et al. [25]. The values h, η and q are obtained from a regression analysis as described previously and have accordingly the dependencies (Eqs. (15), (17), and (18)) as

$$h=h(T^i_{LC},t^i_{LC},T^i_{tg},T^i_{rg},T^i_0,T^i_{tc},G^i),\quad q=q(h),\quad \eta=\eta(h,q) \tag{19}$$

In the following, the absolute error Δx_j of the foregoing variables is considered identical across the different experiments. The following absolute errors can then be computed:

$$\Delta h=\sqrt{\sum_{i=1}^{N}\left[\begin{array}{c}\left(\frac{\partial h}{\partial T^i_{LC}}\Delta T_{LC}\right)^2+\left(\frac{\partial h}{\partial t^i_{LC}}\Delta t_{LC}\right)^2+\left(\frac{\partial h}{\partial T^i_{tg}}\Delta T_{tg}\right)^2+\left(\frac{\partial h}{\partial T^i_{rg}}\Delta T_{rg}\right)^2\\ +\left(\frac{\partial h}{\partial T^i_0}\Delta T_0\right)^2+\left(\frac{\partial h}{\partial T^i_{tc}}\Delta T_{tc}\right)^2+\left(\frac{\partial h}{\partial G^i}\Delta G\right)^2\end{array}\right]}$$

$$\Delta q=\left|\frac{\partial q}{\partial h}\Delta h\right|\Delta\eta=\sqrt{\left(\frac{\partial \eta}{\partial h}\Delta h\right)^2+\left(\frac{\partial \eta}{\partial q}\Delta q\right)^2} \tag{20}$$

A centered scheme is used to approximate the foregoing partial derivatives as

$$\frac{\partial f}{\partial x_j}\approx\frac{f(x_1,\ldots,x_j+\Delta x_j,\ldots,x_J)-f(x_1,\ldots,x_j-\Delta x_j,\ldots,x_J)}{2\Delta x_j}=\frac{\tilde{f}(x_j)}{2\Delta x_j} \tag{21}$$

where x_j, $j=1\ldots J$, are the variables of a function f. The discretization step of the numerical scheme for a given variable is assumed to be identical to the absolute error of this variable and the following is then obtained:

$$\Delta h=\frac{1}{2}\sqrt{\sum_{i=1}^{N}\left[\tilde{h}(T^i_{LC})^2+\tilde{h}(t^i_{LC})^2+\tilde{h}(T^i_{tg})^2+\tilde{h}(T^i_{rg})^2+\tilde{h}(T^i_0)^2+\tilde{h}(T^i_{tc})^2+\tilde{h}(G^i)^2\right]} \tag{22}$$

Subsequently, the errors for q and η become

$$\Delta q=\frac{1}{2}|\tilde{q}(h)|\quad \Delta\eta=\frac{1}{2}\sqrt{\tilde{\eta}(h)^2+\tilde{\eta}(q)^2} \tag{23}$$

A relative error of 1% on the heat flux ratio G is considered. For every temperature measurement, an absolute error of 0.1 K is taken into account. The time detection of the transient liquid crystal signal is based on an absolute error of 0.04 s corresponding to one frame of the video sequence. The error analysis is then based upon a total of nine tests resulting from a combination of three typical coolant gas variations T_{tc} combined with three typical heat flux ratios G.

For the representative result ($h=100\ \mathrm{W/m^2K^{-1}}$, $\eta=0.15$, and $q=1500\ \mathrm{W/m^2}$) of the four experimental cases introduced previously, this leads to a maximum relative error of $<15\%$ on h, of $<3\%$ on η and of $<5\%$ on q. For these conditions, an error analysis on the number of experiments taken into account for the regression shows that there may be an optimum number of coolant gas variations (Fig. 4). In all cases the errors decrease with an increasing number of experiments, albeit to different levels depending on the number of coolant gas variations used. The optimum appears to be for nine experiments issued from a combination of three different coolant gas variations with three different heat flux ratios. This combination of experiments is used for the four test cases presented in this paper.

In addition to the measurement errors, the initial temperature, the liquid crystal temperature, the coolant gas preconditioning levels, and the applied heat fluxes have to be chosen in accordance with the expected values of h, η, and q. This may be assessed using numerical simulations of the temporal evolution of T_w in order to have acceptable t_{LC} values during the experiments. Indeed, a too-fast transient liquid crystal signal leads to higher errors due to a limited time resolution for t_{LC}, and a too-slow transient signals leads also to higher errors as the half-infinite model assumption is no longer satisfied.

5 Results and Discussion

The results shown in the present chapter focus on the effect of different wall boundary conditions (see Fig. 3) on the film cooling performance on a flat plate. It can be seen that for cases 1 and 2, the heat flux distribution at the wall and therefore the wall boundary condition for the film cooling process is different. This is caused by the different connection of the power supply to the heater foil.

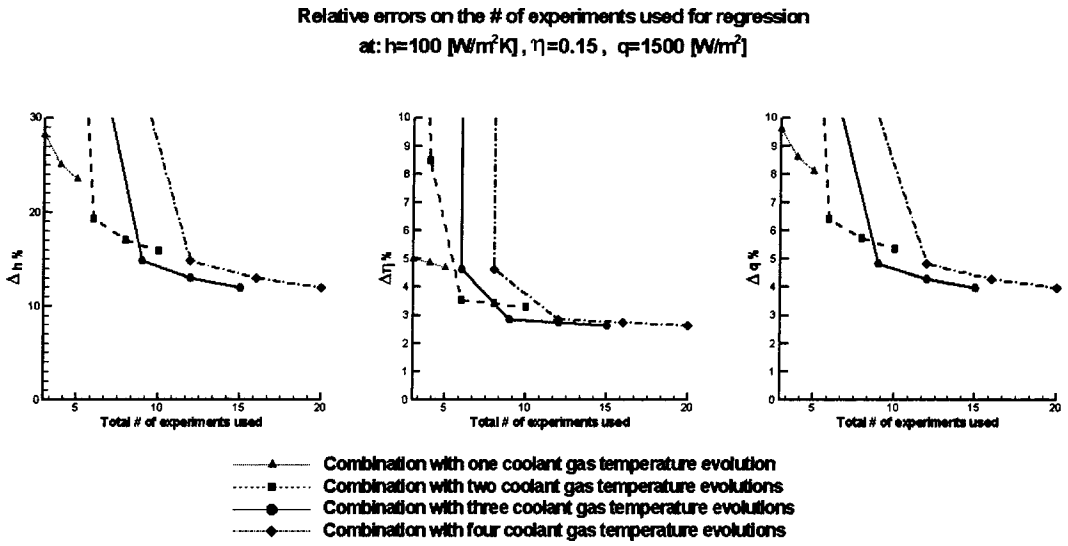

Fig. 4 Relative error evolution with the increase of the number of experiments used for the regression analysis

The reference heat flux q obtained by the regression is presented in its non-dimensional form $q/\overline{q}$ in Fig. 5. The effective surface heat flux generation applied during each experiment i is then the product of q by its gain factor G^i. For case 1, the local surface heat flux tends to increase in between the holes and decreases in the longitudinal prolongation of the holes. The opposite is true for case 2 where the local surface heat flux is low or close to zero in between the holes and increases in their longitudinal prolongation. This corresponds to the expected result when considering the local surface resistance of the foil and the path of the electrical current. The surface heat flux distributions in these two cases have been compared to numerical simulations done using a method described by Wiedner et al. [26]. It is only based on the heater-foil geometry with constant boundary conditions applied on

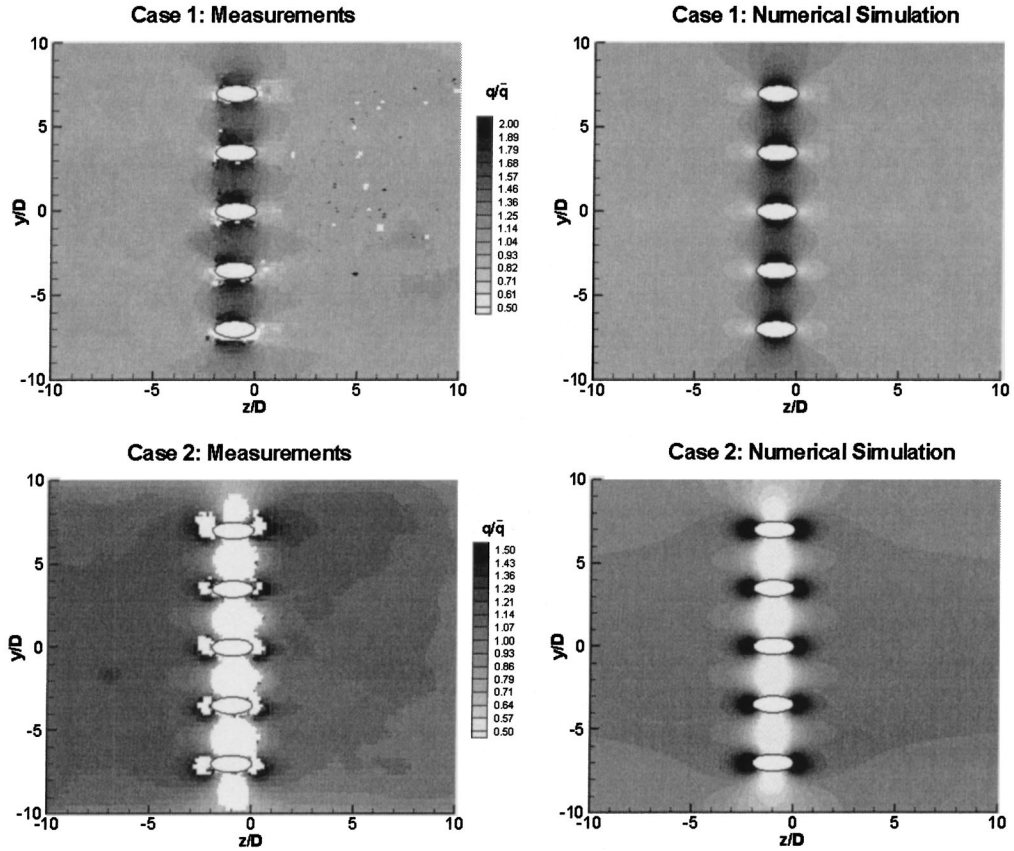

Fig. 5 From measurements derived (left) and calculated (right) dimensionless reference heat flux distribution for cases 1 and 2

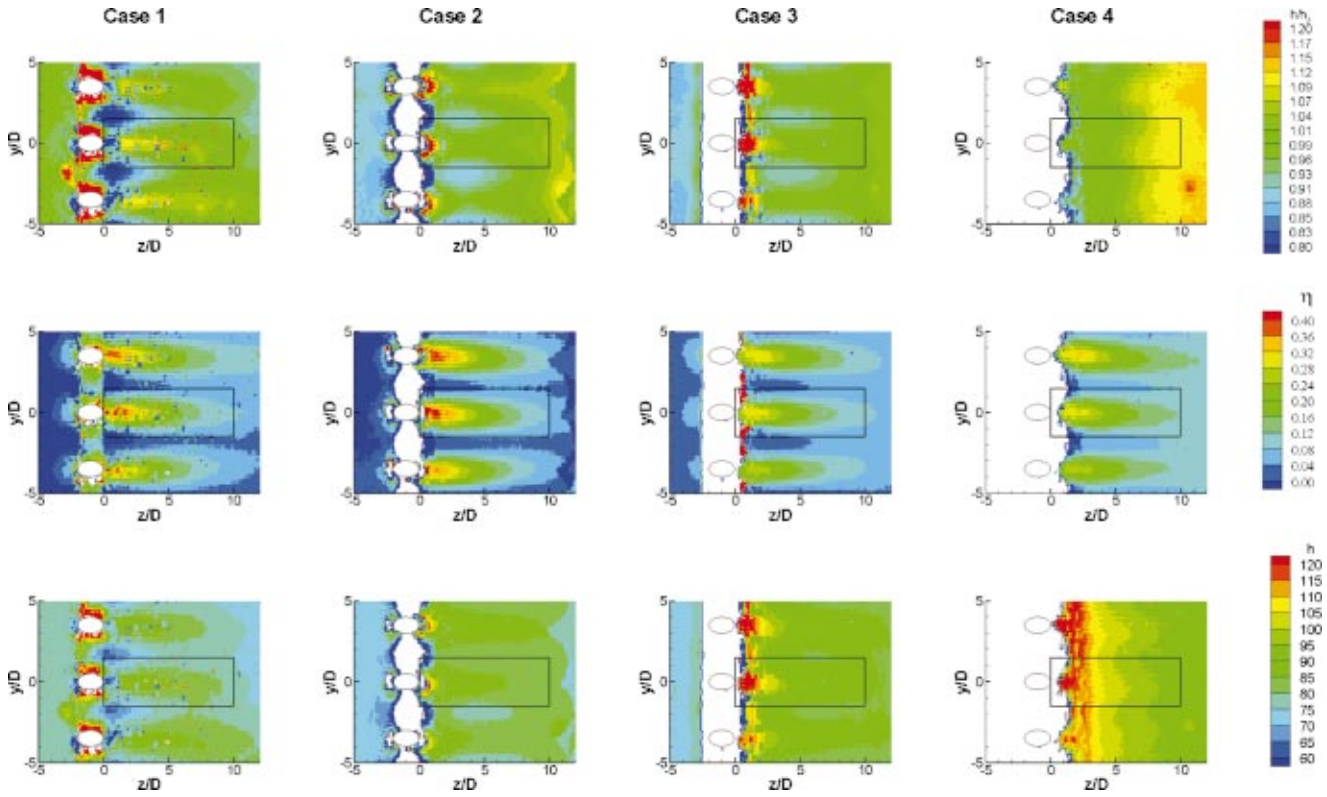

Fig. 6 Spatial distributions of heat transfer coefficients and adiabatic film cooling effectiveness

the bus bars location in order to simulate the electrical current. The resulting simulated heat flux distribution values are also shown in Fig. 5 and present excellent agreement with the experimental values. Hence, they validate the regression approach of multiple transient heater-foil experiments and the development of the new measurement technique described in the foregoing regarding the heat flux determination. Notice that with this measurement technique, the heat flux losses (electrical wiring, lateral conduction) are automatically accounted for without an explicit knowledge of them. These losses have been determined by assessing the difference between the power given by the power supply and the surface heat yielding a difference of ~25%. About 15% are due to the electrical wiring and 10% to lateral conduction effects.

Figure 6 shows the spatial distribution of the heat transfer coefficient and the film-cooling effectiveness for the four heater foil configurations. Additionally the figure shows the heat transfer coefficient ratio h/h_0, where the reference heat transfer coefficient h_0 is based on the value without blowing. If one focuses on the distribution of the heat transfer coefficients, one might see changes in the heat transfer distribution because of the changed thermal boundary conditions between the individual cases. If the near hole region is not taken into account (as there might be some heat conduction effects for $-2<z/D<1$), the difference between the heat transfer coefficients of case 1 and case 2 is quite small and can be generally neglected. This can be explained by the fact that the only difference for these two configurations is the different application of the power supply in order to produce the surface heat flux distribution, yielding a slight change in the thermal boundary layer. However, both configurations lead to the same starting point of the thermal boundary layer. Therefore, the total difference in heat transfer coefficient for a turbulent flowing fluid with a Prandtl number of around one (air) should not be too large. In contrast to these two cases, bigger differences in the heat transfer coefficients can be seen by comparing case 1 with case 3 or case 4. In case 4, the start of the thermal boundary layer is delayed to after the film cooling holes. This results in much higher heat transfer coefficients after the row of holes than in case 1. In case 3, the area between the film-cooling holes is not heated. Also this configuration shows differences in the heat transfer coefficient compared to case 1, the differences being mainly restricted to a near-hole area of about two to four hole diameters. This can be explained by the fact that the disruption in heat flux from the surface to the flow changes only locally the thermal boundary layer thickness for case 3. By relating the heat transfer coefficient to its value without blowing, it seems that smaller differences are present between the individual cases, the biggest differences appearing again between case 4 and the other cases. Focusing finally on the distribution of the adiabatic film-cooling effectiveness, one sees that only very small differences between the individual cases can be observed.

For nearly all design work for film-cooled gas turbine blades, laterally averaged values of the heat transfer coefficients and the film cooling effectiveness play a very important role. Therefore, the results have been laterally averaged for the rectangular area shown in the individual plots of Fig. 6, the results being displayed in Fig. 7. If one focuses on the distribution of the heat transfer coefficients, it is obvious that the heat transfer coefficients from case 4 show the largest deviation to all other cases. For the latter, the change in thermal boundary conditions on the heat transfer coefficients might be neglected. This is an important outcome of the present study, because there are several film-cooling studies known in literature which have used wall boundary conditions similar to case 3. However, the results for the heat transfer coefficients for case 4 show that care has to be taken in selecting appropriate thermal wall boundary conditions for film-cooling experiments. On the other hand, the lateral film-cooling effectiveness values show quite a good agreement for all different wall boundary conditions. Additionally, Fig. 7 shows for the film cooling effectiveness also values from a correlation given by Baldauf et al. [27] based on a large set of experimental data. As can be

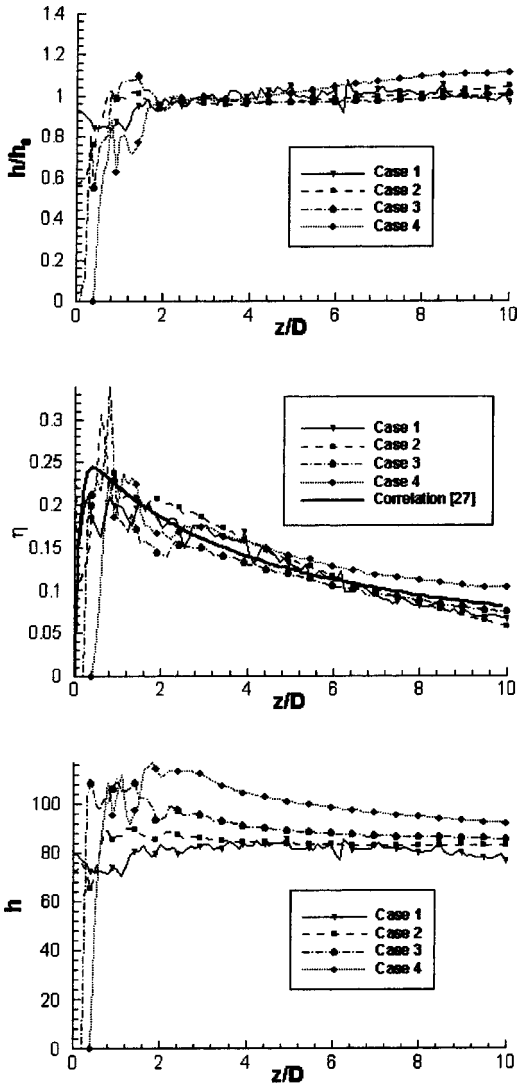

Fig. 7 Lateral-averaged values of the heat transfer coefficient and the adiabatic film-cooling effectiveness (derived from the data given in Fig. 6)

seen, the results obtained here are in good agreement with those found in literature, further validating the present measurement method.

6 Conclusions

The present paper introduces a novel method for determining the heat transfer coefficient and film-cooling effectiveness. This method is based on the liquid crystal technique applied on a heater-foil with film-cooling holes. The method does not need to take into account the surface heat flux distribution and is therefore independent from the power supply configuration and other factors like the variations in thickness and resistance of the heater foil.

In the present paper four different heater-foil configurations have been considered in order to study the influence of the thermal wall boundary conditions on the heat transfer performance of a film-cooled plate. It has been shown that care has to be taken when doing film-cooling experiments since there is a noticeable influence of the thermal wall boundary conditions on the heat transfer coefficients. The present method has been validated against data taken from literature and good agreement has been found.

Nomenclature

a,b,c,d = experimental interpolation parameters, (K, s^{-1}, Ks^{-1}, $Ks^{-1/2}$)
BR = blowing rate $(\rho_c U_c)/(\rho_g U_g)$, (-)
c_p = specific heat at constant pressure, $(J\,kg^{-1}\,K^{-1})$
D = hole diameter, (m)
G = gain factor or heat flux ratio
h = convective heat transfer coefficient, $(W\,m^{-2}\,K^{-1})$
h_0 = convective heat transfer coefficient without coolant injection, $(W\,m^{-2}\,K^{-1})$
k = thermal conductivity of the plate, $(W\,m^{-1}\,K^{-1})$
L_d = hole length, (m)
N = no. of experiments
P = pitch hole, (m)
q = reference wall heat flux, $(W\,m^{-2})$
$\overline{q}$ = average reference wall heat flux, $(W\,m^{-2})$
$\dot{q}_w$ = wall heat flux, $(W\,m^{-2})$
r = index of summation
s = Laplace variable corresponding to t, (s^{-1})
T = temperature, (K)
t = time, (s)
U = flow velocity, $(m\,s^{-1})$
x = axial coordinate, (m)
y = pitchwise coordinate, (m)
z = spanwise coordinate, (m)
α = thermal diffusivity, $(m^2\,s^{-1})$
δ = plate thickness, (m)
ε = error function
η = adiabatic film-cooling effectiveness
ρ = mass density of plate, $(kg\,m^{-3})$

Superscript

i = index of experiment

Subscripts

0 = initial condition
aw = adiabatic wall
c = for coolant gas
g = for main gas
LC = liquid crystals
rg = main gas recovery condition
tc = coolant gas total conditions
tg = main gas total conditions
w = wall $(x=0)$

Abbreviations

CCD = charge-coupled device
LED = light emitting diode

References

[1] Goldstein, R. J., 1971, "Film Cooling," *Advances in Heat Transfer*, eds., T. F. Irvine and J. P. Hartnett, Academic Press, New York, Vol. 7, pp. 321–379.
[2] VKI Lecture Series, 1982, "Film Cooling and Turbine Blade Heat Transfer," VKI-LS 82-02.
[3] Leontiev, A. I., 1999, "Heat and Mass Transfer Problems for Film Cooling," ASME J. Heat Transfer, **121**, pp. 509–527.
[4] Sinha, A. K., Bogard, D. G., and Crawford, M. E., 1990, "Film Cooling Effectiveness Downstream of a Single Row of Holes with Variable Density Ratio," 90-GT-43.
[5] Forth, C. J., Loftus, P. J., and Jones, T. V., 1980, "The Effect of Density Ratio on the Film Cooling of a Flat Plate," AGARD CP 390, Bergen.
[6] Ito, S., Goldstein, R. J., and Eckert, E. R. G., 1978, "Film Cooling of a Gas Turbine Blade," ASME J. Eng. Power, **100**, pp. 476–481.
[7] Takeishi, K., Aoki, S., Sato, T., and Tsukagoshi, K., 1992, "Film Cooling on a Gas Turbine Rotor Blade," ASME J. Turbomach., **114**, pp. 828–834.
[8] Drost, U., 1998, "An Experimental Investigation of Gas Turbine Airfoil Aero-Thermal Film Cooling Performance," thesis N°1817, EPF Lausanne, Switzerland.
[9] Crawford, M. E., 1986, "Simulation Codes for Calculation of Heat Transfer to Convectively Cooled Turbine Blades," VKI-LS, Convective Heat Transfer and Film Cooling in Turbomachinery.
[10] Weigand, B., Bonhoff, B., and Ferguson, J., 1997, "A Comparative Study Between 2D Boundary Layer Predictions and 3D Navier-Stokes Calculations

for a Film Cooled Vane,'' Proc., U.S. National Heat Transfer Conference, Baltimore, HTD 350, pp. 213–221.
[11] Garg, V. K., 1997, ''Comparison of Predicted and Experimental Heat Transfer on a Film-Cooled Rotating Blade using a Two-Equation Turbulence Model,'' 97-GT-220.
[12] Ireland, P. T., and Jones, T. V., 2000, ''Liquid Crystal Measurements of Heat Transfer and Surface Shear Stress,'' Meas. Sci. Technol., **11**, pp. 969–985.
[13] Lutum, E., von Wolfersdorf, J., Weigand, B., and Semmler, K., 2000, ''Film Cooling on a Convex Surface with Zero Pressure Gradient Flow,'' Int. J. Heat Mass Transfer, **43**, pp. 2973–2987.
[14] Reiss, H., 1998, ''The Transient Liquid Crystal Technique Employed for Sub- and Transonic Heat Transfer and Film Cooling Measurements in a Linear Cascade,'' 14th bi-annual symposium on Measurement Techniques in Transonic and Supersonic Flow in Cascades and Turbomachines.
[15] Dui, H., Han, J. C., and Ekkad, V., 1997, ''Detailed Film Cooling Measurements Over a Gas Turbine Blade Using a Transient Liquid Crystal Image Technique,'' HTD 350, National Heat Transfer Conference, **12**.
[16] von Wolfersdorf, J., Hoecker, R., and Sattelmayer, T., 1993, ''A Hybrid Transient Step-Heating Heat Transfer Measurement Technique Using Heater Foils and Liquid-Crystal Thermography,'' ASME J. Heat Transfer, **115**, pp. 319–324.
[17] Turnbull, W. N., and Oosthuizen, P. H., 1999, ''A New Experimental Technique for Measuring Surface Heat Transfer Coefficients Using Uncalibrated Liquid Crystals,'' ASME HTD-Vol. 364-4, pp. 121–126.
[18] Farmer, J. P., Seager, D. J., and Liburdy, J. A., 1997, ''The Effect of Shaping Inclined Slots on Film Cooling Effectiveness and Heat Transfer Coefficient,'' ASME 97-GT-339.
[19] Seager, D. J., and Liburdy, J. A., 1997, ''Experimental Investigation of the Effects of Compound-Angle Holes on Film Cooling Effectiveness and Heat Transfer Performance Using a Transient Liquid Crystal Thermometry Technique,'' *Optical Technology in Fluid, Thermal and Combustion Flow III*, SPIE, **3172**, pp. 173–182.
[20] Vogel, G., Graf, A., and Weigand, B., 2002, ''Film Cooling: A Comparative Study of Different Heater-Foil Configurations for Liquid Crystal Experiments,'' ASME GT-2002-30552.
[21] Vogel, G., and Weigand, B., 2001, ''A New Evaluation Method for Transient Liquid Crystal Experiments,'' NHTC01-1511, 35th ASME National Heat Transfer Conference, Anaheim, CA.
[22] Carslaw, H. S., and Jaeger, J. C., 1959, *Conduction of Heat in Solids*. Oxford University Press, London, Second Edition. Chapter XII and Appendices II & V.
[23] Isaacson, E., and Keller, H. B., 1966, *Analysis of Numerical Methods*, Dover Publications.
[24] Vogel, G., and Bölcs, A., 2000, ''A Novel Digital Image Processing System for the Transient Liquid Crystal Technique applied for Heat Transfer and Film Cooling Measurements,'' ICHMT Paper, Turbine 2000 Symposium, Cesme, Turkey.
[25] Kline, S. J., and McClintock, F. A., 1953, ''Describing Uncertainties in Single-Sample Experiments,'' J. Mech. Eng., Jan., pp. 3–8.
[26] Wiedner, B. G., and Camci, C., 1996, ''Determination of Convective Heat Flux on Steady-State Heat Transfer Surface With Arbitrarily Specified Boundaries,'' ASME J. Heat Transfer, **118**, pp. 850–856.
[27] Baldauf, S., Schulz, A., Wittig, S., and Schleurlen, M., 1997, ''An Overall Correlation of Film Cooling Effectiveness from One Row of Holes,'' 97-GT-79.